

1 **Late Pliocene marine $p\text{CO}_2$ reconstructions from the Subarctic Pacific Ocean**

2 **G. E. A. Swann¹, C. P. Kendrick², and A. J. Dickson³, Savannah Worne¹**

3 ¹School of Geography, University of Nottingham, University Park, Nottingham, NG7 2RD, UK

4 ²NERC Isotope Geosciences Facility, British Geological Survey, Keyworth, Nottingham, NG12
5 5GG, UK

6 ³Department of Earth Sciences, Royal Holloway, University of London, Egham, Surrey, TW20
7 0EX, UK.

8 Corresponding author: George Swann (george.swann@nottingham.ac.uk)

9 **Key Points:**

- 10 • Subarctic Pacific Ocean carbon dynamics reconstructed using diatom carbon isotopes
- 11 • Net ocean-atmosphere CO_2 flux does not alter over the onset of major Northern
- 12 Hemisphere Glaciation (c. 2.75-2.73 Ma).

13 Abstract

14 The development of large ice-sheets across the Northern Hemisphere during the late Pliocene
15 and the emergence of the glacial-interglacial cycles that punctuate the Quaternary mark a
16 significant threshold in Earth's climate history. Although a number of different mechanisms have
17 been proposed to initiate this cooling and the onset of major Northern Hemisphere glaciation,
18 reductions in atmospheric concentrations of CO₂ likely played a key role. The emergence of a
19 stratified (halocline) water column in the subarctic north-west Pacific Ocean at 2.73 Ma has
20 often been interpreted as an event which would have limited oceanic ventilation of CO₂ to the
21 atmosphere, thereby helping to cool the global climate system. Here, diatom carbon isotopes
22 ($\delta^{13}\text{C}_{\text{diatom}}$) are used to reconstruct changes in regional carbon dynamics through this interval.
23 Results show that the development of a salinity stratification did not fundamentally alter the net
24 oceanic/atmospheric flux of CO₂ in the subarctic north-west Pacific Ocean through the late
25 Pliocene/early Quaternary. These results provide further insights into the long-term controls on
26 global carbon cycling and the role of the subarctic Pacific Ocean in instigating global climatic
27 changes.

28 1 Introduction

29 Understanding the processes associated with the progressive Late Pliocene glaciation of
30 the Northern Hemisphere remains an essential objective for understanding the long-term
31 functionality and temporal variability of the global climate system (Mudelsee and Raymo, 2005).
32 Of particular note is the transition associated with the onset of major Northern Hemisphere
33 Glaciation (oNHG) and its intensification (iNHG) from c. 2.75-2.73 Ma onwards in MIS G6
34 when significant ice-sheets developed across Greenland, Eurasia and Northern America (Raymo
35 et al., 1994; Maslin et al., 1996; Kleiven et al., 2002; Matthiessen et al., 2009; Bailey et al.,
36 2013). Instrumental to this transition are Late Pliocene changes in solar insolation, tectonic
37 uplift, water column stratification and the opening/closure of oceanic gateways, all of which
38 triggered oceanic/atmospheric feedbacks that initiated cooler conditions and the increased supply
39 of moisture to high-latitude continental regions (Ruddiman and Kutzbach, 1989; Driscoll and
40 Haug, 1998; Haug and Tiedemann, 1998; Maslin et al., 1998; Ravelo et al., 2004; Sarnthein et
41 al., 2009; Brierley and Fedorov, 2016).

42 The extent to which variations in atmospheric $p\text{CO}_2$ ($p\text{CO}_{2(\text{atm})}$) played a role in triggering
43 both the oNHG and iNHG remains unconstrained. Ocean-atmospheric models have
44 demonstrated that reductions in $p\text{CO}_{2(\text{atm})}$ were probably critical in both instigating and sustaining
45 the development of large ice-sheets through the oNHG (Lunt et al., 2008, 2010; Bonelli et al.,
46 2009; Frank et al., 2010; Willeit et al., 2015), a view supported by most but not all $p\text{CO}_{2(\text{atm})}$
47 reconstructions (e.g., Pagani et al., 2010; Seki et al., 2010; van de Wal et al., 2011; Badger et al.,
48 2013; Martínez-Botí et al. 2015; Willeit et al., 2015; Stap et al., 2016). With any significant
49 change in $p\text{CO}_{2(\text{atm})}$ likely linked to oceanic-atmosphere exchanges, a need exists to identify and
50 evaluate possible marine sources/sinks of CO₂ through the late Pliocene.

51 1.1 Subarctic north-west Pacific Ocean

52 The subarctic north-west Pacific Ocean (Fig. 1) is one location that may have
53 experienced significant changes in ocean-atmospheric carbon dynamics through the late Pliocene
54 and iNHG. Today the subarctic north-west Pacific Ocean acts as a net sink of atmospheric CO₂
55 due to a halocline driven stratification at a depth of c. 150-200 m that minimizes deep water

56 exposure at the ocean-atmosphere interface (Tabata, 1975; Honda et al., 2002; Chierici et al.,
 57 2006) (Fig. 1). Proxy-data records from ODP Site 882 indicate that the halocline developed over
 58 the iNHG at 2.73 Ma with increases in surface freshwater transforming the mixed water column
 59 to a stratified system (Sigman et al., 2004; Haug et al., 2005; Swann et al., 2006; Swann, 2010).
 60 This development altered regional biogeochemical cycling (Reynolds et al., 2008; Shimada et al.,
 61 2009; Bailey et al., 2011; Studer et al., 2012; Swann et al., 2016) with a drop in opal mass
 62 accumulation rates (MAR) from c. 3 g cm⁻² ka⁻¹ to <1 g cm⁻² ka⁻¹ at 2.73 Ma (Haug et al., 1999;
 63 Sigman et al., 2004).

64 These changes observed in the subarctic North Pacific Ocean may also have dramatically
 65 impacted ocean-atmosphere exchanges of CO₂. With the deep North Pacific Ocean enriched in
 66 CO₂ relative to other ocean basins with dissolved inorganic carbon at >2,300 μmol kg⁻¹ (Lauvset
 67 et al. 2016), a mixed water column prior to 2.73 Ma characterized by deep water upwelling may
 68 have ventilated CO₂ to the atmosphere, thereby helping to maintain the warm Pliocene climatic
 69 state (Haug et al., 1999). The emergence of a halocline from 2.73 Ma would have then
 70 minimized such exchanges, transforming the region to a net sink of atmospheric CO₂ similar to
 71 the modern day. This alteration in the direction of net ocean-atmosphere CO₂ exchange would
 72 have aided the iNHG and the global shift to colder climatic conditions (Haug et al., 1999). In an
 73 attempt to constrain the role of the subarctic Pacific in regulating the global climate system and
 74 *p*CO_{2(atm)} in the Piacenzian (3.60-2.58 Ma), diatom carbon isotopes (δ¹³C_{diatom}) are employed to
 75 reconstruct carbon dynamics in the subarctic north-west Pacific Ocean and assess their response
 76 to the expansion of ice sheets across the Northern Hemisphere over the iNHG and the transition
 77 to a stratified water column.

78 1.2 Reconstructing *p*CO₂ from δ¹³C_{diatom}

79 Hitherto, estimates of marine *p*CO₂ (*p*CO_{2(aq)}) and *p*CO_{2(atm)} have been derived from the
 80 boron isotopes (δ¹¹B) of foraminifera (Foster and Rae, 2016), the δ¹³C composition of alkenones
 81 (Pagani, 2002), B/Ca measurements in foraminifera (Yu et al., 2007), fossil leaf stomata (Bai et
 82 al., 2015) and pedogenic carbonate (Montañez et al., 2016). Although each approach contains
 83 uncertainties and assumptions, the combination of approaches together with model simulations
 84 (van de Wal et al. 2011; Stap et al. 2016) are providing increasing consensus on the magnitude of
 85 past *p*CO_{2(atm)} and on the drivers, responses and climate sensitivity of the earth system.

86 Emerging work has promoted the use of δ¹³C_{diatom} to reconstruct *p*CO_{2(atm)} (Heureux and
 87 Rickaby, 2015; Mejía et al., 2017; Stoll et al., 2017). The intrinsic organic carbon matter in
 88 diatoms frustules is comprised of proteins and polyamines that forms a key template for diatom
 89 biomineralisation (Hecky et al., 1973; Swift and Wheeler, 1992; Kröger et al., 1999, 2000;
 90 Sumper and Kröger, 2004). During the photosynthetic production of this organic matter, diatoms
 91 preferentially fractionate ¹²C over ¹³C with the isotopic composition of δ¹³C_{diatom}:

$$92 \quad \delta^{13}C_{diatom} = \delta^{13}C_{DIC} - \epsilon_p - (\epsilon_f - \epsilon_p) \frac{C_i}{C_e} \quad 93$$

94 (Eq. 1)

95 where δ¹³C_{DIC} is the isotopic value of the Dissolved Inorganic Carbon (DIC) substrate; ε_p
 96 is the isotopic fractionation for the diffusion of carbon into the cell; ε_f is the isotopic fractionation
 97 associated with carbon capture by the photosynthetic enzyme RuBisCO having been constrained
 98 at +25‰ by Bidigare et al. (1997) and where C_i and C_e are the intra- and extra-cellular
 99 concentrations of CO₂ in the water column (CO_{2(aq)}) (Laws et al., 1995; Rau et al., 1996, 1997).

100 Accordingly, $\delta^{13}\text{C}_{\text{diatom}}$ can be linked to factors including changes in: 1) $\delta^{13}\text{C}_{\text{DIC}}$ arising from
 101 changes in ocean circulation and the production/dissolution of carbonate producers; 2) photic
 102 zone $p\text{CO}_{2(\text{aq})}$ with increases (decreases) triggering a corresponding decrease (increase) in
 103 $\delta^{13}\text{C}_{\text{diatom}}$ through modification of $C_i:C_e$; and 3) photosynthetic carbon demand with increases
 104 causing a ^{12}C depletion in ambient seawater and so increasing $\delta^{13}\text{C}_{\text{diatom}}$. Attempts to reconstruct
 105 $p\text{CO}_{2(\text{aq})}$ have mainly focused on ϵ_p (the fractionation between diatom bound carbon and $\text{CO}_{2(\text{aq})}$):

$$\epsilon_p = \left[\frac{\delta^{13}\text{C}_{\text{CO}_{2(\text{aq})}} + 1000}{\delta^{13}\text{C}_{\text{diatom}} + 1000} - 1 \right] \cdot 10^3$$

(Eq. 2)

109 In turn, $\delta^{13}\text{C}_{\text{CO}_{2(\text{aq})}}$ can be calculated from the $\delta^{13}\text{C}$ of planktonic carbonate ($\delta^{13}\text{C}_{\text{carbonate}}$),
 110 such as a planktonic foraminifera, building on the temperature-dependent fractionation between
 111 HCO_3^- and $\text{CO}_{2(\text{aq})}$ at a given sea surface temperature (T) (Mook et al., 1974; Romanek et al.,
 112 1992):

$$\delta^{13}\text{C}_{\text{CO}_{2(\text{aq})}} = \left(\frac{\epsilon_{\text{CO}_{2(\text{aq})}-\text{CO}_{2(\text{g})}} + 1}{1000} \right) \cdot (\delta^{13}\text{C}_{\text{CO}_{2(\text{g})}} + 1000) - 1000$$

(Eq. 3)

$$\epsilon_{\text{CO}_{2(\text{aq})}-\text{CO}_{2(\text{g})}} = \frac{-373}{T + 273.15} + 0.19$$

(Eq. 4)

$$\delta^{13}\text{C}_{\text{CO}_{2(\text{g})}} = \frac{\delta^{13}\text{C}_{\text{carbonate}} + 1000}{\epsilon_{\text{calcite}-\text{CO}_{2(\text{aq})}} / 1000 + 1}$$

(Eq. 5)

$$\epsilon_{\text{calcite}-\text{CO}_{2(\text{g})}} = 11.98 - 0.12T$$

(Eq. 6)

124 By targeting marine sediments in which both diatoms and planktonic foraminifera are
 125 preserved in the sediment record, $\delta^{13}\text{C}_{\text{diatom}}$ and $\delta^{13}\text{C}_{\text{foram}}$ can be combined to obtain absolute
 126 values of $\text{CO}_{2(\text{aq})}$ in the ambient photic zone waters:

$$\text{CO}_{2(\text{aq})} = \frac{b}{\epsilon_f - \epsilon_p}$$

(Eq. 7)

130 where ϵ_f is the isotopic fractionation during carbon fixation which has been constrained
 131 as 25‰ (Bidigare et al., 1997) and b is the combination of physiological factors relating to cell
 132 size and growth rate. From this relationship, $p\text{CO}_{2(\text{aq})}$ can be calculated using Henry's law via the
 133 solubility coefficient K_H (Weiss 1970, 1974):

$$p\text{CO}_{2(\text{aq})} = \frac{\text{CO}_{2(\text{aq})}}{K_H}$$

(Eq. 8)

137 from which differences between $p\text{CO}_{2(\text{aq})}$ and $p\text{CO}_{2(\text{atm})}$ can be calculated as:

$$\Delta p\text{CO}_2 = p\text{CO}_{2(\text{aq})} - p\text{CO}_{2(\text{atm})}$$

139

(Eq. 9)

140 In instances where equilibrium exists between the surface ocean and the atmosphere,
 141 $\Delta p\text{CO}_2$ should be zero. Where the two systems are not in equilibrium $\Delta p\text{CO}_2$ provides insights
 142 into the net exchange between the two systems with positive (negative) values of $\Delta p\text{CO}_2$
 143 indicating the marine system acts a source (sink) of atmospheric CO_2 .

144 An advantage in using $\delta^{13}\text{C}_{\text{diatom}}$ to reconstruct $p\text{CO}_{2(\text{aq})}$ is the widespread abundance of
 145 well preserved diatoms in sediments across the globe, particularly in polar regions where
 146 carbonates are not readily preserved. However, whilst clear evidence exists that diatom carbon
 147 fixation is linked to $\text{CO}_{2(\text{aq})}$ (Popp et al. 1998; Rosenthal et al., 2000), reconstructions of $p\text{CO}_{2(\text{aq})}$
 148 require robust estimates of b that accounts for physiological fractionation effects in $\delta^{13}\text{C}_{\text{diatom}}$
 149 including those related to growth rate and cell size (Bidigare et al., 1997; Laws et al., 1995,
 150 2002). For example, alkenone $\delta^{13}\text{C}$ reconstructions of $p\text{CO}_{2(\text{aq})}$ rely on the strong relationship
 151 between b and PO_4^{3-} concentrations in the modern water column (Bidigare et al. 1997; Pagani et
 152 al., 2005). Recent work has demonstrated a strong link between b in diatoms and measures of
 153 productivity/growth rate such as opal concentrations, thereby allowing reconstructions of
 154 $p\text{CO}_{2(\text{aq})}$ from $\delta^{13}\text{C}_{\text{diatom}}$ (Heureux and Rickaby, 2015; Stoll et al., 2017).

155 2 Methods

156 ODP Site 882 lies at the western section of the Detroit Seamounts (50°220N, 167°360E)
 157 in the open waters of the north-west Pacific Ocean at a water depth of 3,244 m (Fig. 1). Samples
 158 from 2.85-2.55 Ma that have previously been analyzed for diatom $\delta^{18}\text{O}$ ($\delta^{18}\text{O}_{\text{diatom}}$) and $\delta^{30}\text{Si}$
 159 ($\delta^{30}\text{Si}_{\text{diatom}}$) (Haug et al., 2005; Swann et al. 2006; Swann 2010, Bailey et al., 2011), using an age
 160 model derived from the astronomical calibration of high resolution GRAPE density and magnetic
 161 susceptibility measurements (Tiedemann and Haug, 1995), were re-analyzed for $\delta^{13}\text{C}_{\text{diatom}}$.
 162 Samples were previously cleaned and prepared for isotope analysis using standard
 163 methodologies for diatom isotope research involving chemical treatment with H_2O_2 , HCl and
 164 sieving with sample purity confirmed through light microscopy and SEM (see Swann et al., 2006
 165 for full details). All analyzed samples originated from the 75-150 μm fraction and are
 166 exceptionally well preserved with no signs of dissolution. This fraction is dominated by two taxa,
 167 *Coscinodiscus marginatus* (Ehrenb.) and *Coscinodiscus radiatus* (Ehrenb.), with *C. marginatus*
 168 dominating (c. > 90% relative biovolume abundance) until after the development of the halocline
 169 at 2.73 Ma when *C. radiatus* becomes dominant (see Supplementary Table 1; Fig. 2). Blooms of
 170 *C. marginatus* and *C. radiatus* occur through the year with elevated fluxes in autumn/early
 171 winter (Takahashi, 1986; Takahashi et al., 1996; Onodera et al., 2005). Consequently, the diatom
 172 isotope data obtained here are interpreted as primarily reflecting annually averaged conditions
 173 with a slight bias towards autumn/early winter months. All $\delta^{13}\text{C}_{\text{diatom}}$ analyses were completed
 174 using a Costech elemental analyzer linked to an Optima mass spectrometer via cold trapping at
 175 the NERC Isotope Geoscience Facility at the British Geological Survey (Hurrell et al., 2011).

176 A number of low-resolution foraminifera $\delta^{13}\text{C}$ records exist at ODP Site 882 over the
 177 iNHG (Maslin et al., 1996) and so can be used to monitor the $\delta^{13}\text{C}$ of the HCO_3^- substrate. For
 178 the purpose of this study only the planktonic *Globigerina bulloides* record is used due to its
 179 tendency to mainly calcify in the uppermost section of the water column at depths similar to the
 180 analyzed diatom taxa. For example, data from other available planktonic taxa, including
 181 *Neogloboquadrina pachyderma* (right + left coiling), are not comparable to $\delta^{13}\text{C}_{\text{diatom}}$ due to their
 182 scarcity in the sediment record and/or due to their potential to calcify at lower depths outside the
 183 photic zone. In an attempt to increase the resolution of the *G. bulloides* record, additional

184 samples were picked where possible and analyzed using an Isoprime Multiprep system attached
 185 to a GV Isoprime dual-inlet mass spectrometer as a tracer of $\delta^{13}\text{C}_{\text{DIC}}$. All $\delta^{13}\text{C}_{\text{diatom}}$ and $\delta^{13}\text{C}_{\text{foram}}$
 186 values are expressed on the V-PDB scale by reference to an internal laboratory standard
 187 calibrated against NBS-19 and NBS-22.

188 Other records from ODP Site 882 that are relevant to this study include estimates of sea
 189 surface salinity (SSS) ($\delta^{18}\text{O}_{\text{diatom}}$) and sea surface temperature (SST) (U_{37}^k) (Haug et al., 2005;
 190 Swann et al., 2006; Swann, 2010) which are required for calculating K_H in Equation 8. Values of
 191 $p\text{CO}_{2(\text{aq})}$ were reconstructed following Equations 1-8 using interpolated values of $\delta^{13}\text{C}_{\text{foram}}$, SST
 192 and SSS with $\delta^{13}\text{C}_{\text{foram}}$ measurements corrected for their offset from $\delta^{13}\text{C}_{\text{DIC}}$ following Spero and
 193 Lea (1996). Estimates of b were derived using existing opal concentrations data (Haug et al.,
 194 1999; Sigman et al., 2004) and calibrations for b published in Stoll et al. (2017) for centric taxa
 195 ($R^2 = 0.86$, $p < 0.01$). The uncertainty associated with b and $p\text{CO}_{2(\text{aq})}$ was calculated using Monte
 196 Carlo simulations (10,000 replicates) with the MonteCarlo package in R (Leschinski et al., 2017;
 197 R Core Team, 2017), assuming a normal distribution for proxy data uncertainty (SSS = 0.3 psu,
 198 SST = 1.2°C) in Equations 1-8.

199 3 Results

200 Analytical reproducibility (1σ) from replicate analysis of sample material was 0.3‰ and
 201 $< 0.1\%$ for $\delta^{13}\text{C}_{\text{diatom}}$, and $\delta^{13}\text{C}_{\text{foram}}$ respectively. Over the analyzed interval through the
 202 Pliocene/early Quaternary, values of $\delta^{13}\text{C}_{\text{diatom}}$ range from -12.9% to -20.8% (Fig. 2,
 203 Supplementary Table 1). From 2.85-2.73 Ma values of $\delta^{13}\text{C}_{\text{diatom}}$ are near constant (mean =
 204 -14.1% , $1\sigma = 0.6\%$). Values of $\delta^{13}\text{C}_{\text{diatom}}$ then decrease for the remainder of the analyzed interval
 205 (mean = -18.0% , $1\sigma = 2.1\%$) in a shift that is concomitant with the marked decline in opal
 206 MAR at ODP Site 882. Through the post-iNHG interval significant variability is apparent in the
 207 $\delta^{13}\text{C}_{\text{diatom}}$ data with recurrent changes of up to 3-4‰ that do not coincide with further changes in
 208 opal MAR. Values of $\delta^{13}\text{C}_{\text{foram}}$ typically range from -0.46% to -0.95% with a shift to marginally
 209 higher values after the iNHG (Fig. 2). Despite efforts to increase the resolution of the $\delta^{13}\text{C}_{\text{foram}}$
 210 record, the number of data points declines after 2.73 Ma with sediments largely free of carbonate
 211 microfossils (Fig. 2).

212 Values of ϵ_p are at or below 5 until 2.73 Ma before increasing to >5 and a mean of 8 (Fig.
 213 3). Reconstructed $p\text{CO}_{2(\text{aq})}$ at ODP Site 882 typically range from c. 225-250 ppm with a peak
 214 value of 314 ppm at 2.81 Ma, a low of 192 ppm at 2.58 Ma and mean uncertainties of 39.5 ppm
 215 (1σ) (Fig. 3, Supplementary Table 1). From 2.85-2.73 Ma $p\text{CO}_{2(\text{aq})}$ displays a long-term decline
 216 from c. 280 ppm to c. 230 ppm ($\bar{x} = 247$ ppm; $1\sigma = 25$ ppm). Thereafter, from 2.71-2.55 Ma,
 217 $p\text{CO}_{2(\text{aq})}$ show a marked increase in variability with fluctuation of 20-60 ppm over the interval (\bar{x}
 218 = 225 ppm; $1\sigma = 28$ ppm).

219

220 4 Discussion

221 4.1 Changes in photic zone $p\text{CO}_{2(\text{aq})}$

222 High values of $\delta^{30}\text{Si}_{\text{diatom}}$ and opal MAR from 2.85-2.73 Ma indicate significant upwelling
 223 of nutrient-rich sub-surface waters which resulted in a productive water column marked by high
 224 rates of silicic acid [$\text{Si}(\text{OH})_4$] utilization (Haug et al., 1999; Sigman et al., 2004; Reynolds et al.,
 225 2008; Bailey et al., 2011; Swann et al., 2016) (Fig. 3). This situation contrasts with the post-2.73

226 Ma interval when the development of a halocline ceased significant upwelling and led to
227 associated reductions in Si(OH)_4 utilization and siliceous productivity (Haug et al., 1999, 2005;
228 Sigman et al., 2004; Swann et al., 2006; Reynolds et al., 2008; Swann et al., 2016) (Fig. 3). The
229 presence of lower $p\text{CO}_{2(\text{aq})}$ after 2.73 Ma is consistent with these palaeoceanographic changes,
230 namely a reduction in deeper CO_2 -rich waters reaching the photic zone under conditions of
231 enhanced near-surface stratification. On this basis, the increased variability of $p\text{CO}_{2(\text{aq})}$ after 2.73
232 Ma may reflect changes in the strength of this stratification, an event which might impact the
233 advection of carbon and nutrient rich deep water supply to the photic zone and so rates of
234 Si(OH)_4 utilization. However, before and after the establishment of the halocline at 2.73 Ma,
235 changes in $p\text{CO}_{2(\text{aq})}$ show no relationship to rates of Si(OH)_4 utilization, SSS or SST (Fig. 3).

236 4.2 Implications for ocean ventilation over the iNHG

237 To establish whether changes in subarctic Pacific $p\text{CO}_{2(\text{aq})}$ resulted in the region acting as
238 a net sink or source of CO_2 , comparisons are needed to estimates of global $p\text{CO}_{2(\text{atm})}$. A number of
239 modeled and proxy-based records have been published in recent years, but here we focus our
240 comparisons on a recent multi-site $\delta^{11}\text{B}$ record which is the highest-resolution record to date and
241 displays a decline in $p\text{CO}_{2(\text{atm})}$ of 40–90 ppm through the late Pliocene/early Pleistocene interval
242 (Martinez-Boti et al., 2015). Calculation of $\Delta p\text{CO}_2$ (Eq. 9) between all $\delta^{13}\text{C}_{\text{diatom}}$ derived $p\text{CO}_{2(\text{aq})}$
243 at ODP Site 882 and interpolated $p\text{CO}_{2(\text{atm})}$ reveals considerable variation over the analyzed
244 interval (Fig. 3). The mean age difference between the interpolated and original $p\text{CO}_{2(\text{atm})}$ data is
245 4.3 ka ($1\sigma = 3.7$ ka). With the exception of one sample at 2.81 Ma, values of $\Delta p\text{CO}_2$ are negative
246 throughout the analyzed interval ($\bar{x} = -68$ ppm; $1\sigma = 43$ ppm). Whilst $\Delta p\text{CO}_2$ is lower after the
247 development of the halocline at 2.73 Ma (pre-2.73 Ma: $\bar{x} = -61$ ppm; $1\sigma = 40$ ppm; post-2.73
248 Ma: $\bar{x} = -78$ ppm; $1\sigma = 47$ ppm), consistent with reduced upwelling of deep waters to the photic
249 zone, this change is not significant ($p = 0.2$). The lack of a systematic shift in mean $\Delta p\text{CO}_2$
250 values after 2.73 Ma can be attributed to the large variations in both $p\text{CO}_{2(\text{aq})}$ and $\Delta p\text{CO}_2$ post-
251 iNHG. More significantly, the results cast doubt on the notion that changes in the regional carbon
252 dynamics in the subarctic Pacific Ocean played a key role in driving the iNHG. Although there is
253 considerable variability in estimates of late Pliocene $p\text{CO}_{2(\text{atm})}$ both within and between individual
254 studies (e.g., Pagani et al., 2010; Seki et al., 2010; Bartoli et al. 2011; van de Wal et al., 2011;
255 Badger et al., 2013; Martínez-Boti et al. 2015; Willeit et al., 2015; Stap et al., 2016) in all cases
256 reconstructed values of $p\text{CO}_{2(\text{atm})}$ remain above typical values of $p\text{CO}_{2(\text{aq})}$ at ODP Site 882. Values
257 of $\Delta p\text{CO}_2$ at ODP Site 882 remains predominantly negative even when considering the Monte
258 Carlo derived uncertainties for both $p\text{CO}_{2(\text{aq})}$ and $p\text{CO}_{2(\text{atm})}$ (Fig. 3).

259 Consistently low values of $\Delta p\text{CO}_2$ from 2.85–2.73 Ma suggest that the mixed water
260 column that prevailed in the Pliocene prior to stratification did not release significant volumes of
261 CO_2 to the atmosphere and so did not help maintain the warm Pliocene climate state. This
262 interval in the ODP Site 882 record is marked by exceptional high opal concentrations of c. 60-
263 75% (c. 2.2–3.2 $\text{g cm}^{-2} \text{ka}^{-1}$) (Haug et al., 1999) and rates of Si(OH)_4 utilization (Swann et al.,
264 2016) (Fig. 3). Consequently, although the mixed water column in this interval would have led to
265 increased delivery of carbon rich waters to the surface, the negative values of $\Delta p\text{CO}_2$ suggest the
266 associated flux of nutrients to the photic zone enabled a highly efficient biological pump that
267 prevented carbon release from the ocean to the atmosphere (Fig. 3, 4a). We note, however, that
268 this scenario is not supported by comparisons to the modern day where regions of strong
269 upwelling and high diatom productivity/export remain net sources of CO_2 to the atmosphere
270 (Takahashi et al., 2009; 2016). The uncertainties in using $\delta^{13}\text{C}_{\text{diatom}}$ to reconstruct $p\text{CO}_{2(\text{aq})}$ are
271 discussed in Section 4.3. Whilst these indicate the issues in quantifying $p\text{CO}_{2(\text{aq})}$ and $\Delta p\text{CO}_2$ from

272 $\delta^{13}\text{C}_{\text{diatom}}$, thereby potentially explaining the anomalous negative values of $\Delta p\text{CO}_2$ at ODP Site
273 882, the underlying trends in $p\text{CO}_{2(\text{aq})}$ and $\Delta p\text{CO}_2$ can be used to understand regional late
274 Pliocene/early Quaternary carbon dynamics in the subarctic Pacific. Although the development
275 of the halocline at 2.73 Ma lowered $p\text{CO}_{2(\text{aq})}$ in line with reduced deep water upwelling, the
276 absence of a bigger decline in $p\text{CO}_{2(\text{aq})}$ as well as $\Delta p\text{CO}_2$ is unexpected. After 2.73 Ma, opal
277 concentration fall to c. 20-33% (c. $0.5\text{-}1.0\text{ g cm}^{-2}\text{ ka}^{-1}$) (Haug et al., 1999; Sigman et al., 2004)
278 with corresponding declines in silicic acid utilization (Swann et al., 2016) (Fig. 3). We argue that
279 a decline in $\text{Si}(\text{OH})_4$ utilization and the efficiency of biological export of carbon balanced out the
280 reduced rate at which deep water carbon was advected to the photic zone, preventing a major
281 decline in $p\text{CO}_{2(\text{aq})}$ or the net flux of CO_2 across the ocean-atmosphere interface ($\Delta p\text{CO}_2$) (Fig.
282 4b).

283 A number of models have indicated that a decline in $p\text{CO}_{2(\text{atm})}$ is critical for the
284 development of large Northern Hemisphere ice-sheets (e.g., Lunt et al., 2008). With evidence
285 presented here that carbon dynamics and $\Delta p\text{CO}_2$ did not significantly change in the subarctic
286 North Pacific Ocean over the iNHG, the focus shifts to the Southern Ocean which plays a key
287 role in regulating the c. 100 ppm variations in $p\text{CO}_{2(\text{atm})}$ over Pleistocene glacial-interglacial
288 cycles (Sigman et al., 2010). Evidence for changes in Antarctic ice-sheet extent together with
289 variations in Southern Ocean sea-ice and stratification through the Pliocene and oNHG
290 (Hillenbrand and Cortese, 2006; Hodell and Venz-Curtis, 2006; Naish et al., 2009; Waddell et al.,
291 2009; McKay et al., 2012) could have enhanced the ability of the Southern Ocean to act as a sink
292 of atmospheric $p\text{CO}_{2(\text{atm})}$ through mechanisms that are analogous to those that occur in the
293 Pleistocene (see Sigman et al., 2010). These processes could have been strengthened by
294 increased aeolian iron deposition in the Southern Ocean over this interval, which would have
295 increased the efficiency of the biological pump and the sequestration of carbon into the ocean
296 interior (Martínez-García et al., 2011).

297 4.3 Uncertainties with $\delta^{13}\text{C}_{\text{diatom}}$

298 Despite measurements of $\delta^{13}\text{C}_{\text{diatom}}$ having been used in palaeoenvironmental
299 reconstructions for over a decade to examine changes in photosynthetic carbon
300 demand/productivity, its use to reconstruct $p\text{CO}_{2(\text{aq})}$ is relatively novel. Consequently, a
301 discussion of the potential errors/limitations with $\delta^{13}\text{C}_{\text{diatom}}$ is appropriate to place the
302 reconstructions of $p\text{CO}_{2(\text{aq})}$ at ODP Site 882 into a wider context.

303 4.3.1 Diatom carbon uptake

304 In contrast to foraminifera formed via the precipitation of HCO_3^- , diatoms uptake carbon
305 from both HCO_3^- and $\text{CO}_{2(\text{aq})}$ through Carbon Concentrating Mechanisms (CCM) which enable
306 the saturation of the enzyme RuBisCO that catalyses carbon fixation (Tortell et al., 1997). Such
307 processes primarily involve either an active, direct, transportation of HCO_3^- and $\text{CO}_{2(\text{aq})}$ into the
308 cell or an indirect HCO_3^- uptake in which an extracellular carbonic anhydrase (eCA) dehydrates
309 HCO_3^- to CO_2 (Sültemeyer et al., 1993; Badger, 2003). In addition to these C_3 photosynthetic
310 pathways, an indirect C_4 pathway has also been identified in which HCO_3^- is converted to malic
311 or aspartic acid and then to CO_2 by decarboxylation (Reinfelder et al., 2000, 2004; Roberts et al.,
312 2007).

313 Results from the Bering Sea, North Pacific, Equatorial Pacific and Southern Oceans show
314 that significant, but variable, amounts of diatom carbon originates from HCO_3^- with the majority
315 of this occurring via direct transportation (Tortell and Morel, 2002; Cassar et al., 2004; Martin

316 and Tortell, 2006, Tortell et al., 2006, 2008, 2010). Although $\text{HCO}_3^-:\text{CO}_{2(\text{aq})}$ uptake ratios may
317 vary with large changes in pH (Trimborn et al., 2008) and inter-species variations in cell
318 morphologies (Martin and Tortell, 2008), others have shown that this ratio does not change with
319 $p\text{CO}_{2(\text{aq})}$, Fe availability, growth rates, primary productivity or frustule area:volume ratios (Cassar
320 et al., 2004; Martin and Tortell, 2006, Tortell et al., 2006, 2008). The results presented here from
321 ODP Site 882 do not account for any isotopic offset that may arise over the usage of HCO_3^- over
322 CO_2 or the potential for active carbon uptake to alter ϵ_p (Burkhardt et al., 2001). For example,
323 increases in $p\text{CO}_{2(\text{aq})}$ have been shown to downregulate CCM (Hennon et al., 2015), introducing a
324 non-linear relationship between ϵ_p and $\delta^{13}\text{C}_{\text{diatom}}$ which impacts the ability to accurately
325 reconstruct changes in $p\text{CO}_{2(\text{aq})}$ (Laws et al., 2002; Raven et al., 2011). Although these issues may
326 impact the absolute values of reconstructed $p\text{CO}_{2(\text{aq})}$, we feel confident given the points made
327 above that changes in $\text{HCO}_3^-:\text{CO}_2$ uptake ratios and transportation mechanism have not
328 significantly altered over the analyzed interval or impacted the underlying trends in $p\text{CO}_{2(\text{aq})}$ and
329 our assertion that the development of the halocline did not fundamentally alter regional carbon
330 dynamics across the iNHG. For example, attempts to reconstruct $p\text{CO}_{2(\text{aq})}$ over the last 14 Ma
331 using models that accounts for diffusive and active uptake of CO_2 by CCM results in different
332 absolute values of $p\text{CO}_{2(\text{aq})}$ but similar temporal trends (Mejía et al., 2017).

333 4.3.2 Physiological factors

334 Physiological controls on the diffusion and fractionation of carbon into diatom,
335 summarized by the term b (Equation 7), may change and alter $\delta^{13}\text{C}_{\text{diatom}}$ in response to different
336 forms of RuBisCO, amino acids, growth rates, cell morphology and CCM (Laws et al., 1995,
337 2002; Rau et al., 1996, 1997, 2001; Rosenthal et al., 2000; Cassar et al., 2006; Scott et al., 2007),
338 which in turn are potentially linked to evidence of a possible inter-species isotope vital effects in
339 fossil measurements of $\delta^{13}\text{C}_{\text{diatom}}$ (Jacot Des Combes et al., 2008).

340 Within the context of this study the impact of isotope vital effects, other
341 symbiont/physiological processes such as diatom cell size, geometry as well as the
342 aforementioned $\text{HCO}_3^-:\text{CO}_2$ uptake process (Laws et al., 1995, 1997; Popp et al., 1998; Jacot des
343 Combes et al., 2008; Martin and Tortell, 2008) can be partially circumvented by the use of a
344 single size fraction of diatoms, dominated by only two taxa (Supplementary Table 1). This point
345 is emphasized from 2.85-2.73 Ma when analyzed samples are dominated by *C. marginatus*
346 (>90% relative abundance) and high nutrient concentrations would have created near-steady
347 photic zone growth rates. Whilst declines in $\delta^{13}\text{C}_{\text{diatom}}$ and b as well as increases in ϵ_p coincide at
348 2.73 Ma with a change from *C. marginatus* to *C. radiatus* dominance in the analyzed samples,
349 we attribute this change to the development of the regional halocline, with concordant changes in
350 SST, SSS and opal concentrations, rather than an inter-species vital effect process (Fig. 2, 3).
351 Whilst modern samples/culture experiments are needed to fully confirm the absence of an inter-
352 species vital effect, we note that values of $\delta^{13}\text{C}_{\text{diatom}}$ both before ($R^2 = 0.01$) and after 2.73 Ma (R^2
353 $= -0.12$) are not related to the relative abundance of either *C. marginatus* or *C. radiatus* despite
354 notable variation in the populations of both taxa in each interval (Supplementary Table 1).
355 Finally, to fully account for physiological processes and reconstruct $p\text{CO}_2$ from $\delta^{13}\text{C}_{\text{diatom}}$,
356 accurate estimates of b are required. Some previous studies have primarily based $p\text{CO}_2$
357 reconstructions from diatoms on growth rates (μ) (e.g., Rosenthal et al., 2000; Heurreux and
358 Rickaby, 2015). Here we elect to directly constrain b based on the results of a Southern Ocean
359 core-top study between the Polar Front and Southern Antarctic Circumpolar Current Front (Stoll
360 et al., 2017). Despite calibrations being statistically significant, the standard error associated with
361 this calibration results in a large uncertainty with the estimates of b used in this study ($1\sigma = 32.3$

362 ± 0.5). This, in turn, is the main source of the uncertainty derived in the Monte Carlo simulations
363 for $p\text{CO}_{2(\text{aq})}$ (Fig. 3). It also remains unknown to what extent the Southern Ocean calibration of b
364 can be directly applied elsewhere in the global ocean, to different taxa and/or through the
365 geological record (Stoll et al., 2017), although these calibrations have been used on samples back
366 to the Miocene (Mejía et al., 2017).

367 4.3.3 Underestimation of $p\text{CO}_{2(\text{aq})}$

368 In addition to the discussion above, we note that the reconstructed values of $p\text{CO}_{2(\text{aq})}$
369 (173-288 ppm) are considerably lower than modern values of $p\text{CO}_{2(\text{aq})}$ (331-408 μatm) from 50-
370 50.5°N and 167-168°E that have been collected over the past two decades in different seasons
371 (Takahashi et al., 2016). The low values are also reflected in the reconstructed values of $\Delta p\text{CO}_2$
372 over the analyzed interval (+15 ppm to -145 ppm; $\bar{x} = -68$ ppm; $1\sigma = 43$ ppm). In contrast,
373 modern monthly $\Delta p\text{CO}_2$ from the region range from -50 μatm to +44 μatm (Takahashi et al.,
374 2009) with mean annual preindustrial $\Delta p\text{CO}_2 + 3$ ppm ($p\text{CO}_{2(\text{aq})} = \text{c. } 280$ ppm; $p\text{CO}_{2(\text{atm})} = \text{c. } 277$)
375 (JAMSTEC, 2013). Although comparing modern and palaeo estimates of $p\text{CO}_{2(\text{aq})}$ and $\Delta p\text{CO}_2$ is
376 problematic given the storage of anthropogenic carbon and warming SST in the modern marine
377 system, these lines of evidences suggest that our $\delta^{13}\text{C}_{\text{diatom}}$ reconstruction might underestimate the
378 true values of $p\text{CO}_{2(\text{aq})}$ and $\Delta p\text{CO}_2$ at ODP Site 882 through the late Pliocene/early Quaternary.
379 Whilst part of this underestimation may relate to differences in $p\text{CO}_{2(\text{aq})}$ seasonality before/after
380 the development of the halocline, the impact of this is likely to be less than the Monte-Carlo
381 inferred uncertainty of the $p\text{CO}_{2(\text{aq})}$ reconstruction (mean uncertainty = 39.5 ppm; see
382 Supplementary Table 1). Given the limited work conducted to date on diatom b and its
383 identification above as the main source of uncertainty in reconstructing $p\text{CO}_{2(\text{aq})}$ in this study, we
384 suggest that further calibrations of this parameter are needed outside of the Southern Ocean and
385 involving a greater range of taxa. Notwithstanding this issue, based on current knowledge we
386 remain confident in the overall trend and magnitude of change in our reconstructed record of
387 $p\text{CO}_{2(\text{aq})}$ and $\Delta p\text{CO}_2$. As such, we reiterate our main finding that the development of the halocline
388 in the subarctic north-west Pacific Ocean at 2.73 Ma did not lead to a major change in regional
389 marine-atmospheric fluxes of CO_2 and that therefore carbon dynamics in the region did not play
390 a major role in aiding the iNHG.

391 5 Conclusions

392 Understanding the potential sources and sinks of atmospheric CO_2 that helped regulate
393 the global climate through the late Pliocene is of critical importance given the interval's potential
394 to act as an analogue for a warmer climate state in the 21st Century and beyond. New results
395 based on $\delta^{13}\text{C}_{\text{diatom}}$ from ODP Site 882 in the north-west subarctic Pacific Ocean show that
396 regional ocean-atmospheric exchanges of CO_2 did not fundamental alter over the iNHG. This
397 occurred despite a reduction in the upwelling of high- $p\text{CO}_{2(\text{aq})}$ deep waters at 2.73 Ma that were
398 balanced by a corresponding reduction in carbon export by a less efficient biological pump.
399 Whilst uncertainties exist in using $\delta^{13}\text{C}_{\text{diatom}}$ to reconstruct $p\text{CO}_{2(\text{aq})}$ and $\Delta p\text{CO}_2$, highlighting the
400 need for more modern calibrations in particular for the term b , the results suggest that any
401 decline in $p\text{CO}_{2(\text{atm})}$ through the late Pliocene and early Quaternary was not driven by changes in
402 the north-west subarctic Pacific Ocean.

403 Acknowledgements, Samples, and Data

404 Supporting data ($\delta^{13}\text{C}_{\text{diatom}}$ and $p\text{CO}_{2(\text{aq})}$ data together with the diatom species composition
405 of analyzed samples from ODP Site 882 between 2.85 Ma and 2.55 Ma) are included as a
406 spreadsheet in the SI. This work was supported by the Natural Environment Research Council
407 and a NERC postdoctoral fellowship award to GEAS (grant numbers NE/F012969/1,
408 NE/F012969/2). We thank the staff at the IODP Gulf Coast Core Repository for providing
409 samples and sampling cores from ODP Site 882 in addition to Carol Arrowsmith for assistance
410 with the $\delta^{13}\text{C}_{\text{diatom}}$ analyses and Hilary Sloane for analyzing the additional planktonic $\delta^{13}\text{C}_{\text{foram}}$
411 samples. Finally, thanks are owed to the two anonymous reviewers and the editor (Stephen
412 Barker) who's comments significantly improved the manuscript.

413 References

- 414 Badger, M. (2003). The roles of carbonic anhydrases in photosynthetic CO_2 concentrating
415 mechanisms. *Photosynthesis Research*, 77, 83-94.
- 416 Badger, M. P. S., Schmidt, D. N., Mackensen, A., & Pancost, R. D. (2013). High-resolution
417 alkenone palaeobarometry indicates relatively stable $p\text{CO}_2$ during the Pliocene (3.3–2.8
418 Ma). *Philosophical Transaction of the Royal Society A*, 371: 20130094.
- 419 Bai, Y.-J., Chen, L.-Q., Ranhotra, P., Wang, Q., Wang, Y.-F., & Li, C.-S. (2015). Reconstructing
420 atmospheric CO_2 during the Plio-Pleistocene transition by fossil *Typha*. *Global Change*
421 *Biology*, 21, 874-881.
- 422 Bailey, I., Liu, Q., Swann, G. E. A., Jiang, Z., Sun, Y., Zhao, X., & Roberts, A. P. (2011). Iron
423 fertilisation and biogeochemical cycles in the sub-Arctic northwest Pacific during the late
424 Pliocene intensification of Northern Hemisphere Glaciation. *Earth and Planetary Science*
425 *Letters*, 307, 253-265.
- 426 Bailey, I., Hole, G. M., Foster, G. L., Wilson, P. A., Storey, C. D., Trueman, C. N., & Raymo,
427 M.E. (2013). An alternative suggestion for the Pliocene onset of major northern
428 hemisphere glaciation based on the geochemical provenance of North Atlantic Ocean ice-
429 rafted debris. *Quaternary Science Reviews*, 75, 181-194.
- 430 Bidigare, R. R., Fluegge, A., Freeman, K. H., Hanson, K. L., Hayes, J. M., Hollander, D., Jasper,
431 J. P., King, L. L., Laws, E. A., Milder, J., Millero, F. J., Pancost, R., Popp, B. N.,
432 Steinberg, P. A., & Wakeham, S. G., Consistent fractionation of ^{13}C in nature and in the
433 laboratory: growth-rate effects in some haptophyte algae. *Global Biogeochemical Cycles*,
434 11, 279-292.
- 435 Bonelli, S., Charbit, S., Kageyama, M., Woillez, M.-N., Ramstein, G., Dumas, C., & Quiquet, A.
436 (2009). Investigating the evolution of major Northern Hemisphere ice sheets during the
437 last glacial-interglacial cycle. *Climate of the Past*, 5, 329-345.
- 438 Brierley, C. M., & Fedorov, A. V. (2016). Comparing the impacts of Miocene–Pliocene changes
439 in inter-ocean gateways on climate: Central American Seaway, Bering Strait, and
440 Indonesia. *Earth and Planetary Science Letters*, 444, 116-130.
- 441 Cassar, N., Laws, E. A., Bidigare, R. R., & Popp, B. N. (2004). Bicarbonate uptake by Southern
442 Ocean phytoplankton. *Global Biogeochemical Cycles*, 18, GB2003,
443 doi:10.1029/2003GB002116 .
- 444 Cassar, N., Laws, E. A., & Popp, B.N. (2006). Carbon isotopic fractionation by the marine
445 diatom *Phaeodactylum tricornutum* under nutrient- and light-limited growth conditions.
446 *Geochimica et Cosmochimica Acta*, 70, 5323-5335.

- 447 Chierici, M., Fransson, A., & Nojiri, Y. (2006). Biogeochemical processes as drivers of surface
448 $f\text{CO}_2$ in contrasting provinces in the subarctic North Pacific Ocean. *Global*
449 *Biogeochemical Cycle*, 20, GB1009, doi: 10.1029/2004GB002356.
- 450 Driscoll, N. W., & Haug, G. H. (1998). A short cut in thermohaline circulation: a cause for
451 Northern Hemisphere Glaciation. *Science*, 282, 436-438.
- 452 Foster, G. L., & Rae, J. W. B. (2016). Reconstructing ocean pH with boron isotopes in
453 foraminifera. *Annual Review of Earth and Planetary Science*, 44, 207-237.
- 454 Frank, D. C., Esper, J., Raible, C. C., Buntgen, U., Trouet, V., Stocker, B., & Joos, F. (2010).
455 Ensemble reconstruction constraints on the global carbon cycle sensitivity to climate.
456 *Nature*, 463, 527-532.
- 457 Haug, G. H., & Tiedemann, R., (1998). Effect of the formation of the Isthmus of Panama on
458 Atlantic Ocean thermohaline circulation. *Nature*, 393, 673-676.
- 459 Haug, G. H., D. M. Sigman, R. Tiedemann, T. F. Pedersen, and M. Sarnthein (1999), Onset of
460 permanent stratification in the subarctic Pacific Ocean, *Nature*, 401, 779-782.
- 461 Haug, G. H., Ganopolski, A., Sigman, D. M., Rosell-Mele, A., Swann, G. E. A., Tiedemann, R.,
462 Jaccard, S., Bollmann, J., Maslin, M. A., Leng, M. J., & Eglinton, G. (2005). North
463 Pacific seasonality and the glaciation of North America 2.7 million years ago. *Nature*,
464 433, 821-825.
- 465 Hecky, R. E., Mopper, K., Kilham, P., & Degens E. T. (1973). The amino acid and sugar
466 composition of diatom cell-walls. *Marine Biology*, 19, 323-331.
- 467 Hennon, G. M. M., Ashworth, J., Groussman, R. D., Berthiaume, C., Morales, R. L., Baliga, N.
468 S., Orellana, M. V., Armbrust, E. V. (2015). Diatom acclimation to elevated CO_2 via
469 cAMP signalling and coordinated gene expression. *Nature Climate Change*. 5, 761-766.
- 470 Heurreux, A. M. C., & Rickaby, R. E. M. (2015). Refining our estimate of atmospheric CO_2
471 across the Eocene–Oligocene climatic transition. *Earth and Planetary Science Letters*.
472 409, 329-338.
- 473 Hillenbrand, C-D., Cortese, G. (2006). Polar stratification: A critical view from the Southern
474 Ocean. *Palaeogeography, Palaeoclimatology, Palaeoecology*, 242, 240-252.
- 475 Hodell, D. A., Venz-Curtis, K. A. (2006). Late Neogene history of deepwater ventilation in the
476 Southern Ocean. *Geochemistry Geophysics Geosystems*, 7, Q09001.
- 477 Honda, M. C., Imai, K., Nojiri, Y., Hoshi, F., Sugawarad, T., & Kusakabe, M. (2002). The
478 biological pump in the northwestern North Pacific based on fluxes and major components
479 of particulate matter obtained by sediment-trap experiments (1997–2000). *Deep-Sea*
480 *Research II*, 49, 5595–5625.
- 481 Hurrell, E. R., Barker, P. A., Leng, M. J., Vane, C. H., Wynn, P., Kendrick, C. P., Verschuren, D.,
482 & Street-Perrott, F. A. (2011). Developing a methodology for carbon isotope analysis of
483 lacustrine diatoms. *Rapid Communications in Mass Spectrometry*. 25, 1567-1574.
- 484 Jacot des Combes, H., Esper, O., De La Rocha, C. L., Abelman, A., Gersonde, R., Yam, R., &
485 Shemesh, A. (2008). Diatom $\delta^{13}\text{C}$, $\delta^{15}\text{N}$, and C/N since the Last Glacial Maximum in the
486 Southern Ocean: Potential Impact of Species Composition. *Paleoceanography*, 23,
487 PA4209, doi:10.1029/2008PA001589.

- 488 JAMSTEC (Japan Agency for Marine-Earth Science and Technology; Atmosphere and Ocean
489 Research Institute; Centre for Climate System Research - National Institute for
490 Environmental Studies) (2013): WCRP CMIP5: The MIROC team MIROC-ESM model
491 output collection. Centre for Environmental Data Analysis, 26th February 2018.
492 <http://catalogue.ceda.ac.uk/uuid/bf3c7e63092b45f2927e3e1d260c4f01>
- 493 Kleiven, H. F., Jansen, E., Fronval, T., & Smith T. M. (2002). Intensification of Northern
494 Hemisphere glaciations in the circum Atlantic region (3.5-2.4 Ma)-Ice-rafted detritus
495 evidence. *Palaeogeography Palaeoclimatology Palaeoecology*, 184, 213-223.
- 496 Kröger, N., Deutzmann, R., & Sumper, M. (1999). Polycationic peptides from diatom biosilica
497 that direct silica nanosphere formation. *Science*, 286, 1129-1132.
- 498 Kröger, N., Deutzmann, R., Bergsdorf, C., & Sumper, M. (2000). Species-specific polyamines
499 from diatoms control silica morphology. *Proceedings of the National Academy of
500 Sciences*, 97, 14,133- 14,138.
- 501 Lauvset, S. K., Key, R. M., Olsen, A., van Heuven, S., Velo, A., Lin, X., Schirnack, C., Kozyr, A.,
502 Tanhua, T., Hoppema, M., Jutterström, S., Steinfeldt, R., Jeansson, E., Ishii, M., Perez, F.
503 F., Suzuki, T., & Watelet, S. (2016). A new global interior ocean mapped climatology: the
504 1° × 1° GLODAP version 2. *Earth System Science Data*, 8, 325-340.
- 505 Laws, E. A., Popp, B. N., Bidigare, R. R., Kennicutt, M. C., & Macko, S. A. (1995). Dependence
506 of phytoplankton carbon isotopic composition on growth rate and [CO₂]_{aq}: theoretical
507 considerations and experimental results. *Geochimica et Cosmochimica Acta*, 59, 1131-
508 1138.
- 509 Laws, E. A., Bidigare, R. R., & Popp, N. B. (1997). Effect of growth rate and CO₂ concentration
510 on carbon isotope fractionation by the marine diatom. *Phaeodactylum tricorutum*,
511 *Limnology and Oceanography*, 42, 1552-1560.
- 512 Laws, E. A., Popp, B. N., Cassar, N., & Tanimoto, J. (2002). ¹³C discrimination patterns in
513 oceanic phytoplankton: likely influence of CO₂ concentrating mechanisms, and
514 implications for palaeoreconstructions. *Functional Planet Biology*, 29, 323-333.
- 515 Leschinski, C. H., (2017). MonteCarlo: Automatic Parallelized Monte Carlo Simulations. R
516 package version 1.0.2. <https://CRAN.R-project.org/package=MonteCarlo>.
- 517 Lunt, D. J., Foster G. L., Haywood, A. M., & Stone, E. J. (2008). Late Pliocene Greenland
518 glaciation controlled by a decline in atmospheric CO₂ levels. *Nature*, 454, 1102-1106.
- 519 Lunt, D. J., Haywood, A. M., Schmidt, G. A., Salzmann, U., Valdes, P. J., & Dowsett, H. J.
520 (2010). Earth system sensitivity inferred from Pliocene modelling and data. *Nature
521 Geosciences*, 3, 60-64.
- 522 McKay, R., Naish, T., Carter, L., Riesselman, C., Dunbar, R., Sjunneskog, C., Winter, D.,
523 Sangiorgi, F., Warren, C., Pagani, M., Schouten, S., Willmott, V., Levy, R., DeConto, R.,
524 Powell, R. D. (2012). Antarctic and Southern Ocean influences on Late Pliocene global
525 cooling. *Proceedings of the National Academy of Sciences of the United States of
526 America*, 109, 6423-6428.
- 527 Martin, C. L., & Tortell, P. D. (2006). Bicarbonate transport and extracellular carbonic anhydrase
528 activity in Bering Sea phytoplankton assemblages: results from isotope disequilibrium
529 experiments. *Limnology and Oceanography*, 51, 2111-2121.

- 530 Martin, C. L., & Tortell, P. D. (2008). Bicarbonate transport and extracellular carbonic anhydrase
531 in marine diatoms. *Physiologia Plantarum*, 133, 106-116.
- 532 Martínez-Boti, M. A., Foster, G. L., Chalk, T. B., Rohling, E. J., Sexton, P. F., Lunt, D. J.,
533 Pancost, R. D., Badger, M. P. S., & Schmidt, D. N. (2015). Plio-Pleistocene climate
534 sensitivity evaluated using high-resolution CO₂ records. *Nature*, 518, 49-54.
- 535 Martínez-García, A., Rosell-Melé, A., Jaccard, S. L., Geibert, W., Sigman, D. M., Haug, G. H.
536 (2011). Southern Ocean dust–climate coupling over the past four million years. *Nature*,
537 476, 312-351.
- 538 Maslin, M. A., Haug, G. H., Sarnthein, M., & Tiedemann, R. (1996). The progressive
539 intensification of northern hemisphere glaciation as seen from the North Pacific.
540 *Geologische Rundschau*, 85, 452-465.
- 541 Maslin, M. A., Li, X-S., Loutre, M-F., & Berger, A. (1998). The contribution of orbital forcing to
542 the progressive intensification of Northern Hemisphere glaciation. *Quaternary Science*
543 *Reviews*, 17, 411-426.
- 544 Matthiessen, J., Knies, J., Vogt, C., & Stein, R. (2009). Pliocene palaeoceanography of the Arctic
545 Ocean and subarctic seas. *Philosophical Transaction of the Royal Society A*, 367, 21-48.
- 546 Mejía, L. M., Méndez-Vicente, A., Abrevaya, L., Lawrence, K. T., Ladlow, C., Bolton, C.,
547 Cacho, I., & Stoll, H. (2017). A diatom record of CO₂ decline since the late Miocene.
548 *Earth and Planetary Science Letters*, 479, 18-33.
- 549 Montañez, I. P., McElwain, J. C., Poulsen, C. J., White, J. D., DiMichele, W. A., Wilson, J. P.,
550 Griggs, G., & Hren, M. T. (2016). Climate, pCO₂ and terrestrial carbon cycle linkages
551 during late Palaeozoic glacial-interglacial cycles. *Nature Geoscience*, 9, 824-828.
- 552 Mook, W. G., Bommerso, J. C., & Staverma, W.H. (1974). Carbon isotope fractionation between
553 dissolved bicarbonate and gaseous carbon-dioxide. *Earth Planet. Sci. Lett*, 22, 169-176.
- 554 Mudelsee, M., & Raymo, M. E. (2005). Slow dynamics of the Northern Hemisphere glaciation.
555 *Paleoceanography*, 20, PA4022, doi:10.1029/2005PA001153.
- 556 Naish, T., Powell, R., Levy, R., Wilson, G., Scherer, R., Talarico, F., Krissek, L., Niessen, F.,
557 Pompilio, M., Wilson, T., Carter, L., DeConto, R., Huybers, P., McKay, R., Pollard, D.,
558 Ross, J., Winter, D., Barrett, P., Browne, G., Cody, R., Cowan, E., Crampton, J., Dunbar,
559 G., Dunbar, N., Florindo, F., Gebhardt, C., Graham, I., Hannah, M., Hansaraj, D.,
560 Harwood, D., Helling, D., Henrys, S., Hinnov, L., Kuhn, G., Kyle, P., Läufer, A.,
561 Maffioli, P., Magens, D., Mandernack, K., McIntosh, W., Millan, C., Morin, R., Ohneiser,
562 C., Paulsen, T., Persico, D., Raine, I., Reed, J., Riesselman, C., Sagnotti, L., Schmitt, D.,
563 Sjunneskog, C., Strong, P., Taviani, M., Vogel, S., Wilch T., Williams, T. (2009).
564 Obliquity-paced Pliocene West Antarctic ice sheet oscillations. *Nature*, 458, 322-328.
- 565 Onodera, J., Takahashi, K., & Honda, M. C. (2005). Pelagic and coastal diatom fluxes and the
566 environmental changes in the northwestern North Pacific during December 1997–May
567 2000. *Deep-Sea Research II*, 52, 2218-2239.
- 568 Pagani, M. (2002). The alkenone-CO₂ proxy and ancient atmospheric carbon dioxide.
569 *Philosophical Transaction of the Royal Society A*, 360, 609-632.
- 570 Pagani, M, Zachos, J. C., Freeman, K. H., Tipple, B., Bohaty, S. (2005). Marked decline in
571 atmospheric carbon dioxide concentrations during the Paleogene. *Science*, 309, 600-603.

- 572 Pagani, M., Liu, Z., LaRiviere, J., & Ravelo, A. C. (2010). High Earth-system climate sensitivity
573 determined from Pliocene carbon dioxide concentrations. *Nature Geosciences*, 3, 27-30.
- 574 Popp, B. N., Laws, E. A., Bidigare, R. R., Dore, J. E., Hanson, K. L., & Wakeham, S. G. (1998).
575 Effect of phytoplankton cell geometry on carbon isotopic fractionation. *Geochimica et*
576 *Cosmochimica Acta*, 62, 69-77.
- 577 R Core Team (2013). R: A language and environment for statistical computing. R Foundation for
578 Statistical Computing, Vienna, Austria. <https://www.R-project.org/>.
- 579 Rau, G. H., Riebesell, U., & Wolf-Gladrow, D. (1996). A model of photosynthetic ^{13}C
580 fractionation by marine phytoplankton based on diffusive molecular CO_2 uptake. *Marine*
581 *Ecology Progress Series*, 133, 275-285.
- 582 Rau, G. H., Riebesell, U., & Wolf-Gladrow, D. (1997). $\text{CO}_{2\text{aq}}$ -dependent photosynthetic ^{13}C
583 fractionation in the ocean: a model versus measurements. *Global Biogeochemical Cycles*,
584 11, 267-278.
- 585 Rau, G. H., Chavez, F. P., & Friederich, G. E. (2001). Plankton $^{13}\text{C}/^{12}\text{C}$ variations in Monterey
586 Bay, California: evidence of non-diffusive inorganic carbon uptake by phytoplankton in
587 an upwelling environment, *Deep-Sea Research I*, 48, 79-94.
- 588 Ravelo, A. C., Andreasen, D. H., Lyle, M., Lyle, A. O. & Wara, M. W. (2004). Regional climate
589 shifts caused by gradual cooling in the Pliocene epoch. *Nature*, 429, 263-267.
- 590 Raven, J., Giordano, M., Beardall, J., Maberly, S. C. (2011). Algal and aquatic plant carbon
591 concentrating mechanisms in relation to environmental change. *Photosynthesis Research*,
592 109, 281-296.
- 593 Raymo, M. E. (1994). The initiation of Northern Hemisphere Glaciation. *Annual Review of*
594 *Earth and Planetary Sciences*, 22, 353-383.
- 595 Reinfelder J. R., Kraepiel, A. M. L., & Morel, F. M. M. (2000). Unicellular C_4 photosynthesis in
596 a marine diatom. *Nature*, 407, 996-999.
- 597 Reinfelder J. R., Milligan, A. J., & Morel, F. M. M. (2004). The role of the C_4 pathway in carbon
598 accumulation and fixation in a marine diatom. *Plant Physiology*, 135, 2106-2111.
- 599 Reynolds B. C., Frank, M., & Halliday, A. N. (2008). Evidence for a major change in silicon
600 cycling in the subarctic North Pacific at 2.73 Ma. *Paleoceanography*, 23, PA4219,
601 doi:10.1029/2007PA001563.
- 602 Roberts, K., Granum, E., Leegood, R. C., & Raven, J. A. (2007). C_3 and C_4 pathways of
603 photosynthetic carbon assimilation in marine diatoms Are under Genetic, not
604 environmental, control, *Plant Physiology*, 145, 230-235.
- 605 Romanek, C. S., Grossman, E. L., & Morse, J. W. (1992). Carbon isotopic fractionation in
606 synthetic aragonite and calcite: effects of temperature and precipitation rate. *Geochimica*
607 *et Cosmochimica Acta*, 56, 419-430.
- 608 Rosenthal, Y., Dahan, M., & Shemesh, A. (2000). Southern Ocean contributions to glacial-
609 interglacial changes of atmospheric $p\text{CO}_2$: an assessment of carbon isotope record in
610 diatoms, *Paleoceanography*, 15, 65-75.
- 611 Ruddiman, W. F., & Kutzbach, J. E. (1989). Forcing of late Cenozoic northern hemisphere
612 climate by plateau uplift in Southern Asia and the American West. *Journal of*
613 *Geophysical Research*, 94, D15, 18,409-18,427.

- 614 Sarnthein, M., Bartoli, G., Prange, M., Schmittner, A., Schneider, B., Weinelt, M., Andersen, N.,
615 & Garbe-Schönberg, D. (2009). Mid-Pliocene shifts in ocean overturning circulation and
616 the onset of Quaternary-style climates, *Climate of the Past*, 5, 269-283.
- 617 Scott, K. M., Henn-Sax, M., Harmer, T. L., Longo, D. L., Frame, C. H., & Cavanaugh, C. M.
618 (2007). Kinetic isotope effect and biochemical characterization of form IA RubisCO from
619 the marine cyanobacterium *Prochlorococcus marinus* MIT9313. *Limnology and*
620 *Oceanography*, 52, 2199-2204.
- 621 Seki, O., Foster, G. L., Schmidt, D. N., Mackensen, A., Kawamura, K., & Pancost, R. D. (2010).
622 Alkenone and boron-based Pliocene $p\text{CO}_2$ records. *Earth and Planetary Science Letters*,
623 292, 201-211.
- 624 Shimada, C., Sato, T., Yamasaki, M., Hasegawa, S., & Tanaka, T. (2009). Drastic change in the
625 late Pliocene subarctic Pacific diatom community associated with the onset of the
626 Northern Hemisphere Glaciation. *Palaeogeography, Palaeoclimatology, Palaeoecology*,
627 279, 207-215.
- 628 Sigman, D. M., Jaccard, S. L., and Haug, G. H. (2004). Polar ocean stratification in a cold
629 climate. *Nature*, 428, 59-63.
- 630 Sigman, D. M., Hain, M. P., Haug, G. H. (2010). The polar ocean and glacial cycles in
631 atmospheric CO_2 concentration. *Nature*, 466, 47-55.
- 632 Spero, H. J., & Lea, D. W. (1996). Experimental determination of stable isotope variability in
633 *Globigerina bulloides*: implications for paleoceanographic reconstructions. *Marine*
634 *Micropaleontology*, 28, 231-246.
- 635 Stap, L. B., de Boer, B., Ziegler, M., Bintanja, R., Lourens, L.J., & van de Wal, R. S. W. (2016).
636 CO_2 over the past 5 million years: Continuous simulation and new $\delta^{11}\text{B}$ -based proxy data.
637 *Earth and Planetary Science Letters*, 439, 1-10.
- 638 Stoll, H. M., Mendez-Vicente, A., Abrevaya, L., Anderson, R. F., Rigual-Hernández, A. S., &
639 Gonzalez-Lemos, S. (2017). Growth rate and size effect on carbon isotopic fractionation
640 in diatom-bound organic matter in recent Southern Ocean sediments. *Earth and*
641 *Planetary Science Letters*, 457, 87-99.
- 642 Studer, A. S., Martínez-García, A., Jaccard, S. L., Girault, F. E., Sigman, D. M., & Haug, G. H.
643 (2012). Enhanced stratification and seasonality in the Subarctic Pacific upon Northern
644 Hemisphere Glaciation-New evidence from diatom-bound nitrogen isotopes, alkenones
645 and archaeal tetraethers. *Earth and Planetary Science Letters*, 351-352, 84-94.
- 646 Sültemeyer, D., Schmidt, C., & Fock, H. P. (1993). Carbonic anhydrases in higher plants and
647 aquatic microorganisms. *Physiologia Plantarum*, 88, 179-190.
- 648 Sumper, M., & Kröger, N. (2004). Silica formation in diatoms: the function of long-chain
649 polyamines and silaffins. *Journal of Materials Chemistry*, 14, 2059-2065.
- 650 Swann, G. E. A. (2010). Salinity changes in the North West Pacific Ocean during the late
651 Pliocene/early Quaternary from 2.73 Ma to 2.53 Ma. *Earth and Planetary Science*
652 *Letters*, 297, 332-338.
- 653 Swann, G. E. A., Maslin, M. A., Leng, M. J., Sloane, H. J., & Haug, G. H. (2006). Diatom $\delta^{18}\text{O}$
654 evidence for the development of the modern halocline system in the subarctic northwest
655 Pacific at the onset of major Northern Hemisphere glaciation. *Paleoceanography*, 21,
656 PA1009, doi:10.1029/2005PA001147.

- 657 Swann, G. E. A., Snelling, A. M., & Pike, J. (2016). Biogeochemical cycling in the Bering Sea
658 over the onset of major Northern Hemisphere Glaciation. *Paleoceanography*, 31, 1261-
659 1269.
- 660 Swift, D. M., & Wheeler, A. P. (1992). Evidence of an organic matrix from diatom biosilica.
661 *Journal of Phycology*, 28, 202 -290.
- 662 Tabata, S. (1975). The general circulation of the Pacific Ocean and a brief account of the
663 oceanographic structure of the North Pacific Ocean. Part I - circulation and volume
664 transport. *Atmosphere*, 13, 133-168.
- 665 Takahashi, K. (1986). Seasonal fluxes of pelagic diatoms in the subarctic Pacific, 1982-1983.
666 *Deep Sea Research Part A*, 33, 1225-1251.
- 667 Takahashi, K., Hisamichi, K., Yanada, M., & Maita, Y. (1996). Seasonal changes of marine
668 phytoplankton productivity: a sediment trap study. *Kaiyo Monthly*, 10, 109-115 [In
669 Japanese].
- 670 Takahashi, T., Sutherland, S. C., Wanninkhof, R., Sweeney, C., Feely, R. A., Chipman, D. W.,
671 Hales, B., Friederich, G., Chavez, F., Watson, A., Bakker, D. C. E., Schuster, U., Metzl,
672 N., Yoshikawa-Inoue, H., Ishii, M., Midorikawa, T., Nojiri, Y., Sabine, C., Olafsson, J.,
673 Arnarson, T. S., Tilbrook, B., Johannessen, T., Olsen, A., Bellerby, R., Körtzinger, A.,
674 Steinhoff, T., Hoppema, M., de Baar, H. J. W., Wong, C. S., Delille, B., & Bates, N. R.
675 (2009). Climatological mean and decadal changes in surface ocean $p\text{CO}_2$, and net sea-air
676 CO_2 flux over the global oceans. *Deep Sea Research Part II*, 554-577.
- 677 Takahashi, T., Sutherland, S. C., & Kozyr, A. (2016). Global Ocean Surface Water Partial
678 Pressure of CO_2 Database: Measurements Performed During 1957-2015 (2015).
679 ORNL/CDIAC-160, NDP-088(V2015). Carbon Dioxide Information Analysis Center,
680 Oak Ridge National Laboratory, U.S. Department of Energy, Oak Ridge, Tennessee, doi:
681 10.3334/CDIAC/OTG.NDP088(V2015).
- 682 Tiedemann, R., & Haug, G. H. (1995). Astronomical calibration of cycle stratigraphy for Site
683 882 in the northwest Pacific, in *Proceedings of the Ocean Drilling Program, Scientific*
684 *Results Volume*, edited by Rea, D. K., Basov, I. A., Scholl, D. W. & Allan, J. F. pp. 283-
685 292, Ocean Drilling Program, College Station, Texas.
- 686 Tortell, P. D., & Morel, F. M. M. (2002). Sources of inorganic carbon for phytoplankton in the
687 eastern Subtropical and equatorial Pacific Ocean. *Limnology and Oceanography*, 47,
688 1012-1022.
- 689 Tortell, P. D., Reinfelder, J. R., & Morel, F. M. M. (1997). Active uptake of bicarbonate by
690 diatoms. *Nature*, 390, 243-244.
- 691 Tortell, P. D., Martin, C. L., & Corkum, M. E. (2006). Inorganic carbon uptake and intracellular
692 assimilation by subarctic Pacific phytoplankton assemblages. *Limnology and*
693 *Oceanography*, 51, 2102-2110.
- 694 Tortell, P. D., Payne, C., Gueguen, C., Strzepek, R. F., Boyd, P. W., & Rost B. (2008). Inorganic
695 carbon uptake by Southern Ocean phytoplankton. *Limnology and Oceanography*, 45,
696 1485-500.
- 697 Tortell, P. D., Trimborn, S., Li, Y., Rost, B., & Payne, C. D. (2010). Inorganic carbon utilization
698 by Ross Sea phytoplankton across natural and experimental CO_2 gradients. *Journal of*
699 *Phycology*, 46, 433-443.

- 700 Trimborn, S., Lundholm, N., Thoms, S., Richter, K-U, Krock, B., Hansen, P. J., & Rost, B.
701 (2008). Inorganic carbon acquisition in potentially toxic and non-toxic diatoms: the effect
702 of pH-induced changes in seawater carbonate chemistry. *Physiologia Plantarum*, 133, 92-
703 105.
- 704 van de Wal, R. S. W., de Boer, B., Lourens, L. J., Köhler, P., & Bintanja, R. (2011).
705 Reconstruction of a continuous high-resolution CO₂ record over the past 20 million years.
706 *Climate of the Past*, 7, 1459-1469.
- 707 Waddell, L. M., Hendy, I. L., Moore, T. C., Lyle, M. W. (2009). Ventilation of the abyssal
708 Southern Ocean during the late Neogene: a new perspective from the subantarctic Pacific.
709 *Paleoceanography*, 24, PA3206.
- 710 Weiss R. F. (1970). The solubility of nitrogen, oxygen and argon in water and seawater. *Deep*
711 *Sea Research*, 17, 721-735.
- 712 Weiss R. F. (1974). Carbon dioxide in water and seawater: the solubility of a non-ideal gas.
713 *Marine Chemistry*, 2, 203-215.
- 714 Willeit, M., Ganopolski, A., Calov, R., Robinson, A., & Maslin, M. (2015). The role of CO₂
715 decline for the onset of Northern Hemisphere glaciation. *Quaternary Science Reviews*,
716 119, 22-34.
- 717 Yu, J., Elderfield, H., & Hönisch, B. (2007). B/Ca in planktonic foraminifera as a proxy for
718 surface seawater pH. *Paleoceanography*, 22, PA2202, doi:10.1029/2006PA001347.
- 719
720
- 721 **Figure 1.** Location of ODP Site 882 (50°22'N, 167°36'E) in the north-west subarctic Pacific
722 Ocean. Colours indicate annual modern gridded surface water pCO_{2(aq)} (Takahashi et al., 2016).
723 Map created using Ocean Data View (<https://odv.awi.de>).
- 724 **Figure 2.** Late Pliocene/early Quaternary palaeoceanographic records from ODP Site 882.
725 Changes in δ¹⁸O_{diatom} derived SSS (Swann et al., 2006; 2010), U^k₃₇ derived SST (Haug et al.,
726 2005), δ¹³C_{foram} (*G. bulloides*) (Maslin et al., 1996, 1998; this study) and δ¹³C_{diatom}, used to
727 reconstruct pCO_{2(aq)} (Equation 1-9), are compared to the relative diatom species biovolume in
728 samples analyzed for δ¹³C_{diatom}. Orange dashed line denotes transition from unstratified to
729 stratified water column at 2.73 Ma with gray (white) shading reflecting glacial (interglacial)
730 intervals.
- 731 **Figure 3.** Temporal changes in carbon dynamics at ODP Site 882. Values of δ¹³C_{diatom}, ε_p, *b* and
732 pCO_{2(aq)} are compared to pCO_{2(atm)} (Martinez-Boti et al., 2015) and used to calculate ΔpCO₂.
733 Shaded polygons for *b*, pCO_{2(aq)}, pCO_{2(atm)} and ΔpCO₂ reflect the 1σ uncertainty derived from
734 Monte-Carlo simulations. Changes in opal concentrations (Haug et al., 1999; Sigman et al.,
735 2004) and rates of Si(OH)₄ utilization (Swann et al., 2016) provide information on the biological
736 pump and the export of carbon into the ocean interior. Orange dashed line denotes transition
737 from unstratified to stratified water column at 2.73 Ma with gray (white) shading reflecting
738 glacial (interglacial) intervals.
- 739 **Figure 4.** Conceptual model of the palaeoceanographic changes in the north-west subarctic
740 Pacific Ocean. A) From 2.85-2.73 Ma an unstratified water column leads to unimpeded
741 upwelling of deep water. The transportation of nutrients and carbon rich waters to the photic

742 zone is compensated by high levels of siliceous productivity and Si(OH)_4 utilization creating a
743 highly efficient biological pump that minimizes CO_2 leakage to the atmosphere. B) Following the
744 development of the halocline, deep waters are limited from reaching the photic zone. The
745 corresponding decline in both the strength and efficiency of the biological pump, however,
746 results in the net ocean-atmospheric flux of CO_2 remaining similar to conditions prior to 2.73 Ma
747 with only minor decreases in $p\text{CO}_{2(\text{aq})}$ and $\Delta p\text{CO}_2$.

Figure 1

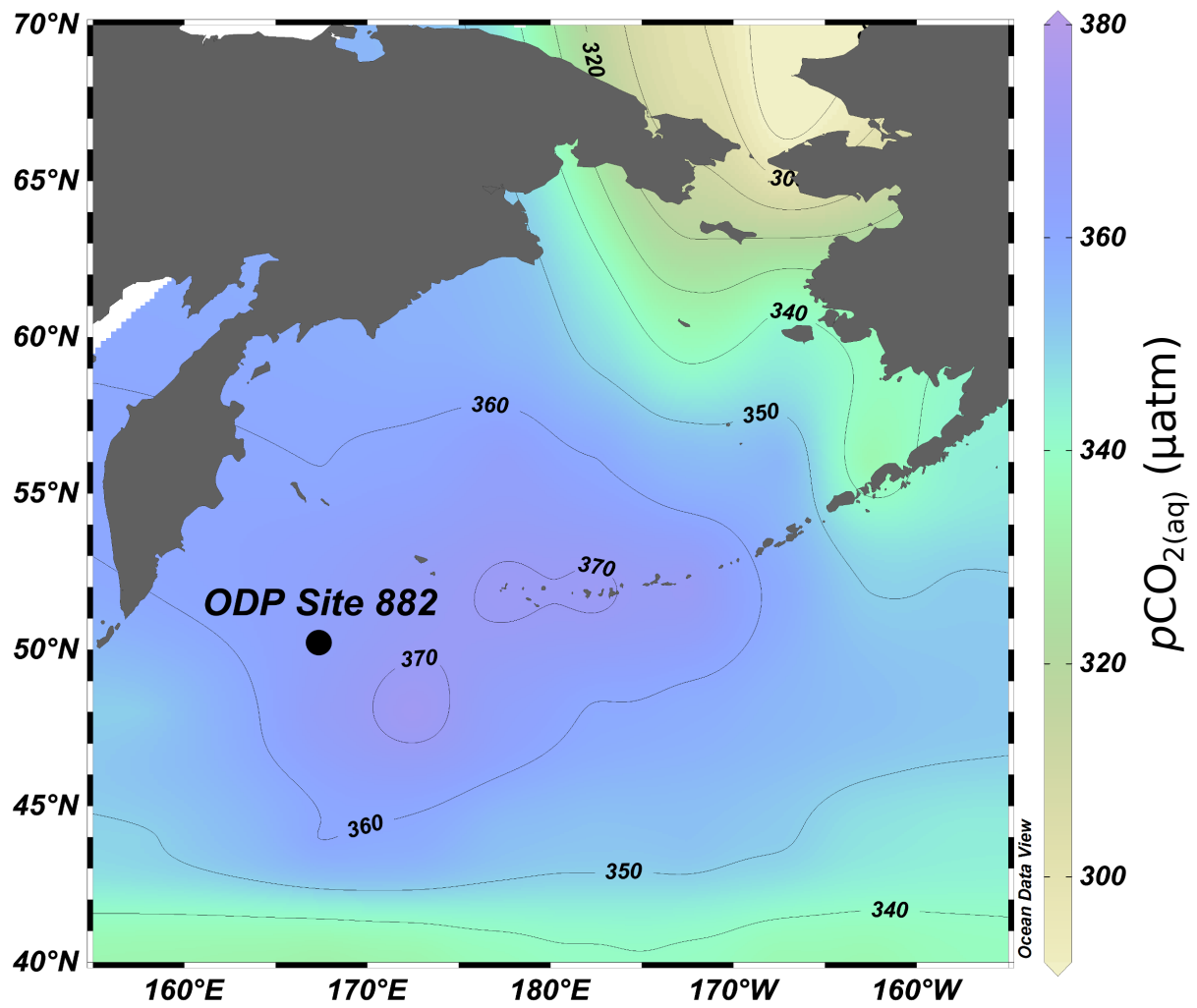


Figure 2

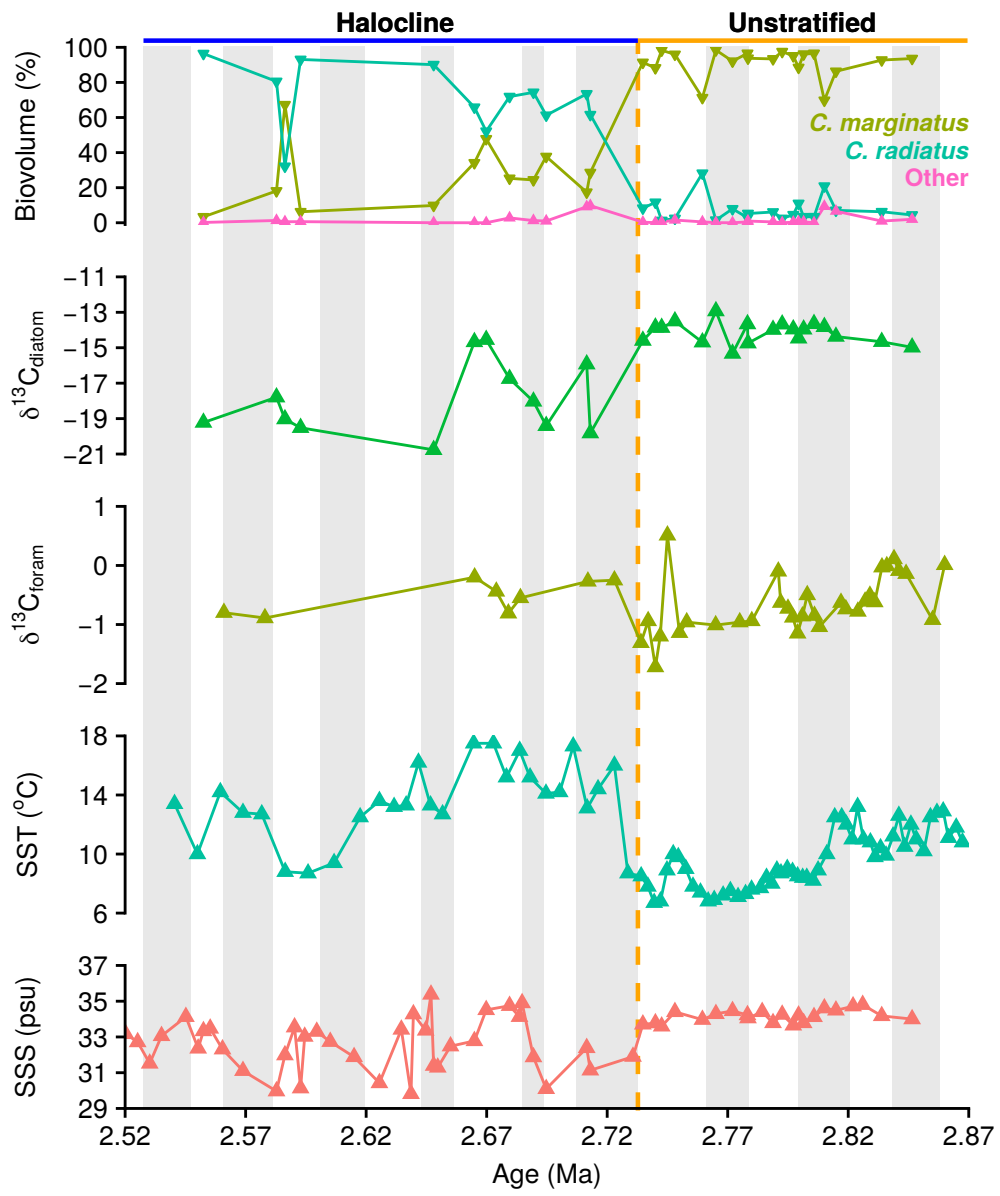


Figure 3

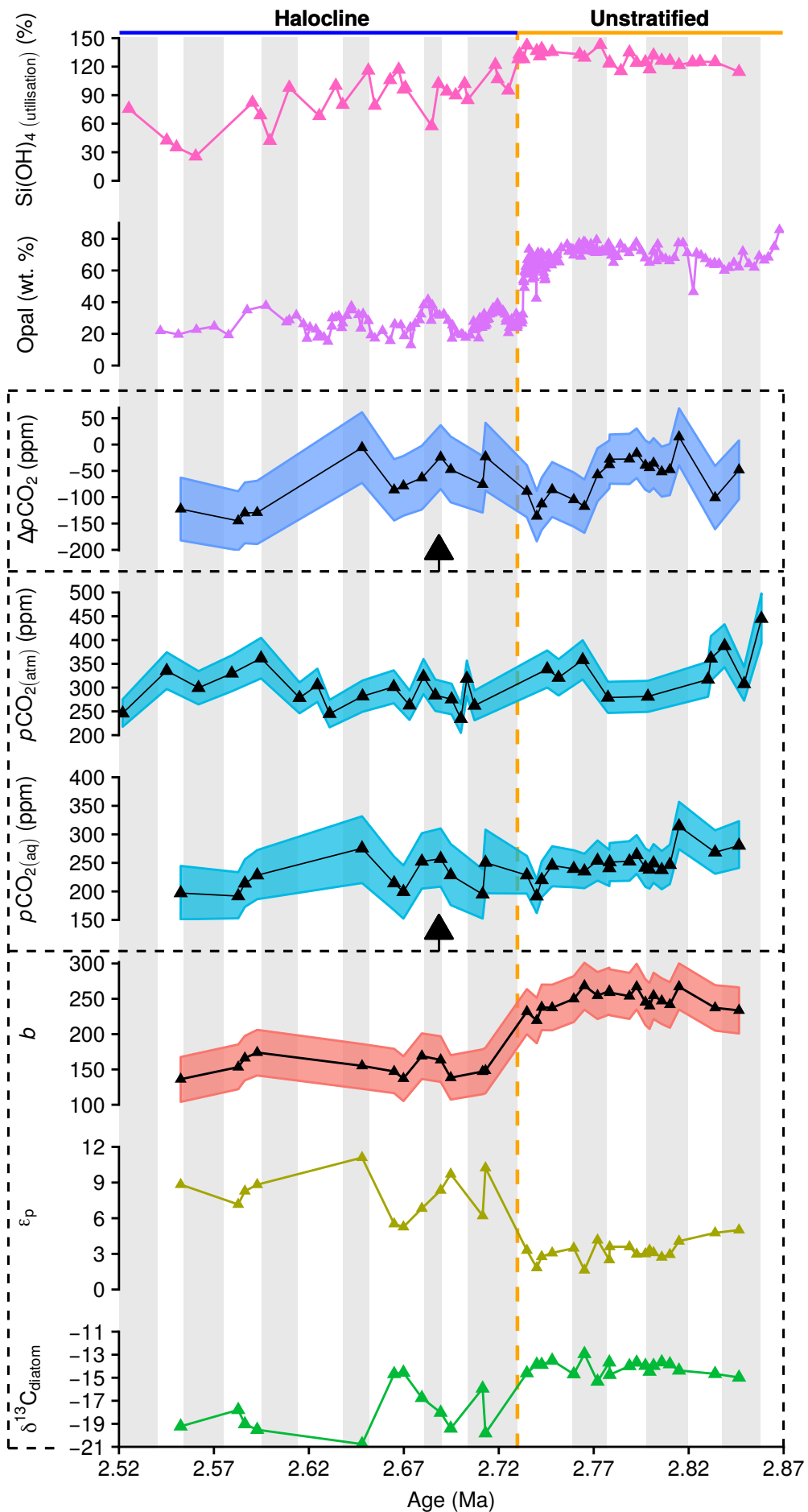


Figure 4

